JOURNAL OF GEOPHYSICAL RESEARCH, VOL. 105, NO. B3, PAGES 5721–5734, MARCH 10, 2000

Contemporary crustal deformation in east Asia constrained by Global Positioning System measurements

Zheng-kang Shen,[1] Chengkun Zhao,[2] An Yin,[1] Yanxing Li,[2] David D. Jackson,[1] Peng Fang,[3] and Danan Dong[4]

Abstract. Global Positioning System (GPS) measurements collected since the early 90's allow us to derive geodetic velocities at 16 permanent stations in east Asia and 68 campaign mode sites in north China. The resulting velocity field shows the following: (1) Contrary to the early inferences that the Shanxi Rift has accommodated significant right-slip motion, our results suggest that the rift system, at least in its northern part in north China, is under ESE-WNW extension at a rate of 4±2 mm/yr. The velocity field also suggests that an ESE-WNW trending left-lateral shear zone deforming at a rate of 2±1 mm/yr may exist along the north rim of north China at the latitude of ~40°N, separating actively extending north China in the south from relatively stable Mongolia in the north. (2) Central and east China move at a rate of 8-11 mm/yr east-southeast with respect to Siberia, implying that the overall east-southeastward motion is the dominant mode of deformation in east China. (3) The India plate moves at a rate of 6±1 mm/yr slower than the NUVEL-1A model prediction relative to the Eurasia plate. (4) Significant eastward motion (20±2 mm/yr) with respect to Siberia occurs in southeastern Tibet. About half of this eastward motion (~11 mm/yr) is absorbed by structures along the eastern boundary of the Tibetan Plateau.

1. Introduction

A prominent feature of east Asian tectonics is widespread Cenozoic deformation caused by the collision between the Indian and Eurasian continents and by the subduction of the Pacific and Philippine Sea Plates beneath Eurasia [*Molnar and Tapponnier*, 1975; *Tapponnier and Molnar*, 1977]. The Indo-Asia collision raised the Tibetan Plateau, uplifted the Himalayan and Tian Shan mountains and created several large-scale strike-slip faults in central and east Asia (Figure 1). The Altyn Tagh Fault along the northwestern edge of the Tibetan Plateau and the Kunlun and Xianshuihe Faults on the north and east sides of the plateau are faults that resulted from north-south shortening and eastward extrusion [*Peltzer et al.*, 1989; *Kidd and Molnar*, 1988; *Allen et al.*, 1991; *Wang et al.*, 1998]. The Qilian Shan Fault, a transpressional structure, may have been created by the eastward extrusion of the Tibetan Plateau [*Gaudemer et al.*, 1995]. North of the plateau, the Ordos block has experienced ESE-WNW extension on its east and west sides associated with a counterclockwise rotation [*State Seismological Bureau Research Group (SSBRG)*, 1988]. Southeast of the plateau, material has been moved south to southeast along the Xianshuihe, Xiaojiang, and Red River Fault systems with respect to the east Himalaya syntaxis in the west and the Sichuan Basin in the east [*Peltzer and Tapponnier*, 1988; *Avouac and Tapponnier*, 1993; *Royden et al.*, 1997; *Wang et al.*, 1998]. In east China, however, in contrast to the proposed eastward extrusion caused by the Indo-Asian collision, regionally active deformation could also have been influenced by the back arc extension [*Northrup et al.*, 1995].

Although the widespread Cenozoic deformation of Asia has been extensively studied, how strain is distributed and evolves with time remains controversial (cf. *Peltzer and Tapponnier*, 1988; *England and Houseman*, 1988; *Houseman and England*, 1993; *England and Molnar*, 1997]. Past investigations have focused on relatively long-term deformation, from thousands to millions of years [e.g., *Armijo et al.*, 1986; *Harrison et al.*, 1992; *Van der Woerd et al.*, 1998; *Ma*, 1987; *Leloup and Kienast*, 1993; *Yin et al.*, 1998]. Owing to large uncertainties in the age of deformation, it is difficult to constrain precisely the contemporary deformation field over a large region such as east Asia by these studies. Various kinematic models have been used to describe crustal deformation in east Asia, but two end-member models have been most intensely debated. *Avouac and Tapponnier* [1993] interpreted geologically determined fault slip rates in the Indo-Asian collision zone with a rigid block motion model. Using an improved data set, *England and Molnar* [1997] approximated the deformation by a spatially continuous strain rate field. Examining historical and instrumental seismic moment data, *Holt et al.* [1995] estimated seismogenic strain accumulation rates in the region, again employing a spatially continuous model. Finite difference or finite element methods have also been used to model the dynamics of the Indo-Asian collision [*Kong and Bird*, 1996; *Peltzer and Saucier*, 1996; *Royden et al.*, 1997]. All those studies, except the regional study by *Royden et al.* [1997] that included geodetic measurements of crustal deformation, relied mainly on geological and seismic data and inevitably suffered from large uncertainties. Owing to those limitations, the answers to fundamental questions related to active east Asia tectonics remain inconclusive. For example, it is not clear

[1]Department of Earth and Space Sciences, University of California, Los Angeles.
[2]First Crustal Deformation Monitoring Center, China Seismological Bureau, Tianjin, China.
[3]Scripps Institution of Oceanography, University of California, San Diego.
[4]Jet Propulsion Laboratory, California Institute of Technology, Pasadena.

Paper number 1999JB900391
0148-0227/00/1999JB900391$09.00

whether the deformation is block-like or distributed in a continuum over a large area.

The GPS technique has provided an effective and unique tool to precisely measure large-scale deformation, as well as deformation along individual faults [*Dixon*, 1991]. Although the spacing of the GPS stations is still sparse in general in Asia, GPS studies grown steadily during the last decade are starting to provide key constraints to the mode of deformation in east Asia [e.g., *King et al.*, 1997; *Bilham et al.*, 1997; *Abdrakhmatov et al.*, 1996; *Larson et al.*, 1999]. This study is another step toward realizing this goal.

2. GPS Data Collection and Analysis

We use three sets of GPS data to investigate crustal deformation in China. The first was collected at permanent stations around the globe. Since 1991, an international consortium, the International GPS Service (IGS), has been coordinating an effort to collect and archive GPS data from continuously recording stations operated by various agencies around the world for global tectonics research [*Neilan*, 1995]. The number of IGS sites has grown steadily over the past 8 years. These fiducial stations have become the backbone sites for precise orbital determination, and also reference sites for regional geodetic surveys.

The First Crustal Deformation Monitoring Center (FCDMC) of the China Seismological Bureau (CSB) has conducted a series of GPS field campaigns in China since 1992. In the north China region they collected data from their North China network using Ashtech L12 receivers in 1992 and from the North China/Capital Circle network using Ashtech Z12 receivers in 1995 and 1996. All the data are included in this study, and the site locations and occupation history are listed in Table 1. A fixed station in Tianjin was surveyed continuously during the 1992 field campaign.

The third data set comes from a permanent Chinese GPS network. Since 1995, the FCDMC, in coordination with a number of Chinese research institutions and government agencies, has established a permanent station network in China and made observations concurrently with the north China field campaigns in 1995 and 1996 and other field surveys in 1997 using Rogue 8000/8100 receivers. These permanent sites, as well as the IGS east Asia stations, are listed in Table 2.

We processed and analyzed the GPS data in three steps. First, we processed the GPS carrier phase data to obtain loosely constrained daily solutions for the station positions and satellite orbits using the GAMIT software [*King and Bock*, 1995] (see *Shen et al.*, [1997] and http://www.scecdc.scec.org/group_e/release.v2 for details of the processing procedure). The 1992 data were processed together with about 20 global IGS stations. A distributed processing approach [*Blewitt et al.*, 1993] was adopted to process the data collected since 1995. The data were divided into three groups: the first includes all the survey mode and permanent sites in east Asia, and each of the other two includes about 35 global IGS sites, respectively. Six IGS stations at Fortaleza (Brazil), Hartebeesthoek (South Africa), Kokee Park (Hawaii), Pasadena (California), Tsukuba (Japan), and Wettzell (Germany) coexist in both IGS processing groups; and nine other IGS sites, Bangalore (India), Irkutsk (Russia), Lhasa (Tibet), Kitab (Uzbekistan), Shanghai (China), Taejon (South Korea), Taipei (Taiwan), Tsukuba and Usuda (Japan), coexist in one of the IGS solutions and the east Asia regional solution. The three separately processed solutions were then combined using the GLOBK software [*Herring*, 1995] by solving commonly shared parameters, such as the satellite orbits and station positions. This processing scheme is efficient while maintaining reasonably homogeneous solutions. In addition to the years when the regional surveys were performed, we also included daily solutions from 1993, 1994, 1998, and 1999 for the global and east Asia permanent sites to help constrain the global reference frame. About 30 days of data for each of the 4 years were used.

Our last step in the processing was to combine all the daily solutions, and model deformation at each station with a constant velocity using the QOCA software [*Dong et al.*, 1998; http://sideshow.jpl.nasa.gov/~dong/qoca]. The combination was done through sequential Kalman filtering, allowing global translation and rotation for each daily solution. Random walk style perturbations were allowed for some parameters whose errors were found correlated with time, such as the Earth rotation parameters and the antenna heights at a few sites. The antenna height errors might be caused by the residual effects of the atmospheric perturbation and pole tide corrections.

We solved for an antenna phase center shift common to all the north China sites after 1992 as well (the same parameters for all the receivers). Introduction of these parameters was necessary because the receivers and antennas used in the 1992 survey (Ashtech L12) were different from those used in the later years (Ashtech Z12), and the early Ashtech units are known to have a phase center offset problem. (The problem was not well known at the time when the surveys were conducted, otherwise the experiments would have been done differently.) We are not aware of studies offering convincing results from mapping the phase centers for the Ashtech L12 and Z12 antennas. Therefore we allowed 3 degrees of freedom in our data modeling to solve for the antenna phase center shifts. Inclusion of the extra parameters for the antenna phase center modeling has resulted in a slight increase of the solution uncertainty. The increase is rather minor because the same parameters are shared by many north China stations and demands very small contribution from each of them.

It has been recognized that error spectra of GPS data are complex. They are spatially correlated because of common orbital, Earth rotation, and regional atmospheric errors [e.g., *Feigl et al.*, 1993]. They are temporally colored because the errors from the atmospheric disturbance, monument instability, and orbital misfits are correlated in time [e.g., *Zhang et al.*, 1997; *Mao et al.*, 1999]. Many conventional approaches for error analysis such as evaluating the RMS for individual station velocities do not work adequately because neither can the errors for individual sites be easily isolated from others nor are they white for a least squares analysis. In this study we followed an error analysis approach of *Dong et al.* [1998]. We first performed the data modeling in an iterative process. In each iteration we used the Kalman filter twice, once forward and once backward. At each step when a data file was added, the increment of the postfit χ^2 due to the addition of the data file and the increase of degrees of freedom in data space were evaluated in a conventional way, and the χ^2 per degree of freedom was calculated. Each data file would then be reweighted after the iteration, so that the total χ^2 from the forward and backward runs for each data file would be close to 2. This procedure gives adequate relative weighting for the individual data files. The next step was to evaluate the increase of the number of parameters caused by allowing the parameter perturbation in the Kalman filtering process. The total RMS would then be reevaluated with an updated estimate of the number of degrees of freedom. The velocity solutions would then be rescaled based on the RMS estimation. For more details of the method, please refer to *Dong et al.* [1998].

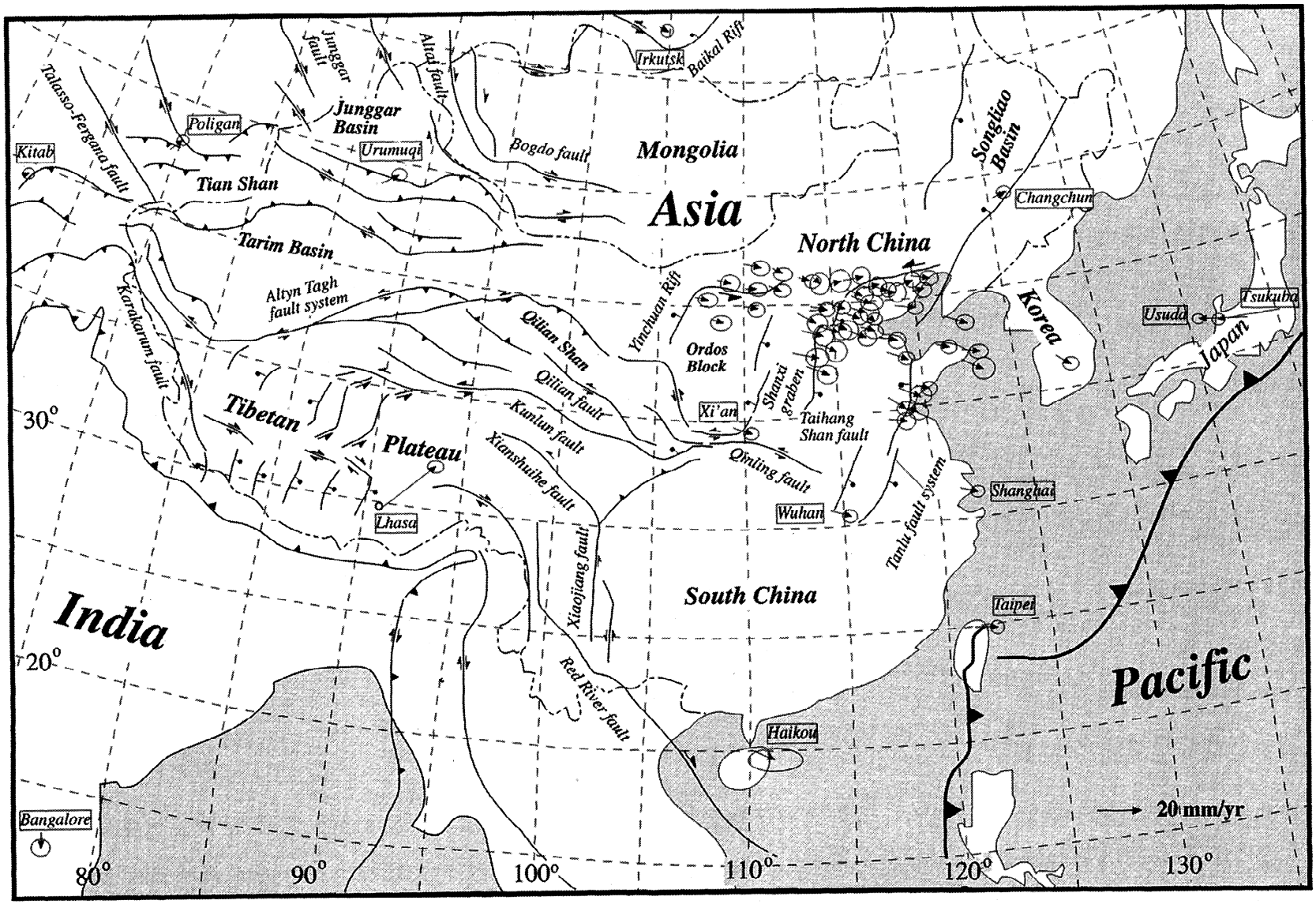

Figure 1. Active tectonic setting and GPS-derived station velocities in east Asia. Solid curves are the major faults in the region, with their thrust, strike-slip, and normal faulting directions indicated by the teeth, arrow pairs, and balls, respectively. Solid arrows are station residual velocities with respect to NNR (No-Net-Rotation) NUVEL-1A. Each arrow originates at the location of the site and points to its motion direction. The error ellipses represent 95% confidence. Some of the station velocities in north China area are not shown here but can be found in a regional figure (Figure 3).

Table 1. North China Campaign Mode Stations and Their Residual Velocities with Respect to NNR NUVEL-1A

Site	Longitude East		Latitude North		East, mm/yr				North, mm/yr				Corr	Occupation
					NNRA	GPS	GPS-NNRA	σ	NNRA	GPS	GPS-NNRA	σ		Year in 1900
G0AB	122°	3'	36°	56'	21.5	30.9	9.4	2.0	-13.2	-18.2	-5.0	1.9	0.00	95,96
G151	114°	55'	40°	43'	22.2	27.4	5.2	2.0	-11.9	-10.5	1.4	2.0	-0.01	95,96
G172	112°	39'	37°	42'	22.7	33.8	11.0	2.0	-11.5	-14.3	-2.8	1.9	-0.03	95,96
G174	113°	22'	37°	4'	22.6	31.9	9.3	1.9	-11.6	-15.3	-3.7	1.7	-0.01	95,96
G178	114°	21'	38°	2'	22.4	28.6	6.2	1.9	-11.8	-15.3	-3.5	1.8	-0.02	95,96
G184	121°	14'	38°	55'	21.4	30.6	9.2	1.6	-13.1	-17.6	-4.5	1.5	0.01	95,96
H001	107°	3'	40°	15'	23.2	28.6	5.4	1.7	-10.3	-11.2	-0.9	1.4	-0.01	92,96
H002	108°	0'	39°	15'	23.1	27.8	4.7	1.8	-10.5	-11.6	-1.1	1.5	-0.01	92,95,96
H003	108°	24'	41°	1'	23.0	28.1	5.1	1.8	-10.6	-11.7	-1.1	1.5	-0.01	92,95,96
H004	109°	57'	41°	45'	22.7	30.0	7.3	1.6	-10.9	-12.5	-1.6	1.3	-0.01	92,95,96
H005	109°	57'	39°	52'	22.9	28.1	5.2	1.6	-10.9	-12.1	-1.2	1.3	-0.01	92,95,96
H006	110°	2'	40°	39'	22.8	28.4	5.6	1.6	-11.0	-11.5	-0.5	1.3	-0.01	92,95,96
H007	111°	26'	40°	45'	22.6	28.4	5.8	1.5	-11.2	-13.1	-1.9	1.3	-0.01	92,95,96
H008	111°	42'	41°	30'	22.5	27.0	4.5	1.6	-11.3	-13.4	-2.1	1.3	-0.03	92,95,96
H010	113°	1'	39°	30'	22.5	31.3	8.8	1.8	-11.6	-16.7	-5.1	1.7	-0.02	95,96
H011	113°	10'	41°	6'	22.4	28.9	6.5	1.5	-11.6	-13.7	-2.1	1.3	-0.03	92,95,96
H012	113°	15'	38°	42'	22.5	32.0	9.5	2.0	-11.6	-14.6	-3.0	1.9	-0.04	95,96
H013	113°	18'	40°	13'	22.4	30.9	8.5	1.5	-11.6	-13.4	-1.8	1.3	-0.02	92,95,96
H014	113°	24'	40°	38'	22.4	29.8	7.4	1.8	-11.6	-11.4	0.2	1.6	-0.02	95,96
H015	113°	39'	39°	3'	22.5	30.6	8.1	1.6	-11.7	-15.1	-3.4	1.4	-0.01	92,95,96
H016	113°	46'	39°	46'	22.4	30.0	7.6	1.5	-11.7	-13.2	-1.5	1.3	-0.02	92,95,96
H017	113°	59'	41°	6'	22.3	25.7	3.4	1.9	-11.8	-14.8	-3.0	1.8	-0.01	95,96
H018	114°	10'	38°	50'	22.4	33.2	10.8	1.8	-11.8	-14.6	-2.8	1.8	-0.01	95,96
H019	114°	13'	39°	25'	22.4	31.1	8.7	1.7	-11.8	-15.7	-3.9	1.7	-0.02	95,96
H020	114°	17'	40°	25'	22.3	29.6	7.3	1.5	-11.8	-13.6	-1.8	1.3	-0.01	92,95,96
H022	114°	43'	39°	54'	22.3	29.2	6.9	1.5	-11.9	-14.3	-2.4	1.3	0.00	92,95,96
H023	114°	44'	39°	20'	22.3	33.5	11.2	1.6	-11.9	-17.2	-5.3	1.4	-0.02	92,95,96
H024	114°	45'	40°	52'	22.2	29.3	7.1	1.8	-11.9	-10.2	1.7	1.7	-0.02	95,96
H025	114°	55'	40°	40'	22.2	27.0	4.8	1.9	-11.9	-10.8	1.1	1.8	-0.01	95,96
H026	115°	3'	38°	54'	22.3	29.2	6.9	1.9	-12.0	-15.0	-3.0	1.6	-0.01	95,96
H027	115°	24'	39°	43'	22.2	28.7	6.5	1.5	-12.0	-13.0	-1.0	1.4	-0.01	95,96
H028	115°	28'	40°	21'	22.1	28.8	6.7	1.5	-12.0	-14.6	-2.6	1.3	0.01	92,95,96
H029	115°	31'	40°	12'	22.1	28.8	6.7	1.7	-12.0	-13.5	-1.5	1.6	-0.01	95,96
H030	115°	36'	39°	28'	22.2	30.5	8.3	1.6	-12.1	-15.6	-3.5	1.3	0.00	92,95,96
H032	115°	49'	39°	39'	22.1	31.5	9.4	1.7	-12.1	-14.4	-2.3	1.7	-0.01	95,96
H034	115°	50'	40°	52'	22.0	29.8	7.8	1.6	-12.1	-10.7	1.4	1.5	-0.01	95,96
H035	115°	52'	38°	35'	22.2	31.8	8.6	1.6	-12.1	-15.9	-3.8	1.5	-0.01	95,96
H036	115°	56'	39°	2'	22.2	30.1	7.9	1.5	-12.1	-14.5	-2.4	1.3	0.00	92,95,96
H037	115°	56'	40°	28'	22.0	29.9	7.9	1.8	-12.1	-14.8	-2.7	1.7	-0.01	95,96
H039	116°	0'	39°	53'	22.1	29.4	7.3	1.8	-12.1	-13.0	-0.9	1.7	-0.01	95,96
H040	116°	2'	39°	47'	22.1	30.5	8.4	1.5	-12.1	-13.7	-1.6	1.3	-0.00	92,95,96
H041	116°	7'	39°	36'	22.1	30.5	8.4	1.8	-12.2	-14.7	-2.5	1.7	-0.01	95,96
H043	116°	14'	40°	11'	22.0	30.7	8.7	1.9	-12.2	-16.1	-3.9	1.5	-0.06	92,95,96
H044	116°	28'	39°	8'	22.1	30.1	8.0	1.6	-12.2	-15.1	-2.9	1.6	-0.01	95,96
H045	116°	35'	38°	41'	22.1	28.2	6.1	1.6	-12.2	-14.7	-2.5	1.5	0.00	95,96
H046	116°	37'	40°	43'	21.9	27.9	6.0	1.5	-12.3	-13.9	-1.6	1.3	-0.02	92,95,96
H048	116°	56'	40°	26'	21.9	28.5	6.6	1.8	-12.3	-12.0	0.3	1.7	-0.00	95,96
H052	117°	19'	39°	40'	21.9	27.6	5.7	1.6	-12.4	-14.6	-2.2	1.4	-0.04	92,95,96
H053	117°	34'	38°	10'	22.0	30.3	8.3	1.5	-12.4	-14.3	-1.9	1.5	0.00	95,96
H054	117°	33'	40°	28'	21.8	28.4	6.6	1.5	-12.4	-14.2	-1.8	1.3	0.01	92,95,96
H055	117°	47'	34°	28'	22.2	30.2	8.0	1.6	-12.5	-13.6	-1.1	1.4	0.03	92,95,96
H056	117°	51'	35°	24'	22.1	29.9	7.8	1.6	-12.5	-17.8	-5.3	1.4	0.03	92,95,96

Table 1. (continued)

Site	Longitude East	Latitude North	East, mm/yr				North, mm/yr				Corr	Occupation
			NNRA	GPS	GPS-NNRA	σ	NNRA	GPS	GPS-NNRA	σ		Year in 1900
H057	117° 51'	39° 21'	21.9	30.1	8.2	1.5	-12.5	-14.2	-1.7	1.5	-0.01	95,96
H058	117° 54'	40° 57'	21.7	26.8	5.1	1.5	-12.5	-14.3	-1.8	1.4	-0.00	95,96
H059	117° 58'	37° 28'	22.0	30.7	8.7	1.5	-12.5	-15.4	-2.9	1.3	0.01	92,95,96
H060	118° 7'	39° 43'	21.8	28.6	6.8	1.6	-12.5	-14.8	-2.3	1.4	0.01	92,95
H061	118° 11'	35° 5'	22.1	32.5	10.4	1.9	-12.5	-16.5	-4.0	1.5	0.07	92,95,96
H062	118° 14'	40° 11'	21.8	26.8	5.0	1.8	-12.5	-13.0	-0.5	1.7	0.00	95,96
H064	118° 28'	35° 50'	22.0	31.4	9.4	1.9	-12.6	-16.7	-4.1	1.5	0.07	92,95,96
H066	118° 42'	39° 32'	21.7	30.8	9.1	1.5	-12.6	-14.0	-1.4	1.3	0.00	95,96
H068	118° 54'	40° 25'	21.6	28.8	7.2	1.5	-12.7	-10.4	2.3	1.4	0.00	95,96
H070	119° 23'	35° 53'	21.9	28.0	6.1	1.5	-12.8	-15.0	-2.2	1.3	0.02	92,95,96
H071	119° 46'	40° 45'	21.5	29.5	8.0	1.6	-12.8	-14.0	-1.2	1.6	0.01	95,96
H072	119° 49'	40° 4'	21.5	26.5	5.0	1.5	-12.8	-12.6	-0.2	1.3	0.03	92,95,96
H074	120° 42'	37° 47'	21.6	27.9	6.3	1.5	-13.0	-14.5	-1.5	1.3	0.01	92,95,96
H078	122° 9'	37° 23'	21.4	29.3	7.9	1.5	-13.2	-15.5	-2.3	1.3	0.01	92,95,96

NNRA, NNR NUVEL-1A model predictions; GPS, GPS solutions; GPS-NNRA, solutions with respect to NNR NUVEL-1A predictions, i.e., with respect to the stable Eurasia plate for all the sites expect IISC, which is with respect to the India plate; σ, uncertainties; Corr, correlation between east and north velocity components.

We constrained the reference frame of our velocity solution to a global plate model of NNR (No-Net-Rotation) NUVEL-1A [*DeMets et al.*, 1990; *Argus and Gordon*, 1991; *DeMets et al.*, 1994]. *Larson et al.* [1997] compared GPS derived station velocities for a group of IGS stations with the NNR NUVEL-1A model predictions and found very good consistency for most of the sites located in Europe, North and South America, Australia, Africa, and Antarctica. We therefore constrained a group of IGS site velocities whose horizontal components show < 2 mm/yr departure from the NNR NUVEL-1A model predictions in *Larson et al.*'s [1997] study. Those sites (listed in Table 3 of *Larson et al.* [1997]) are ALGO (Algonquin, Canada) and FAIR (Fairbank, Alaska) of North America, KOUR (Kourou, French Guyana) of South America, KOSG (Kootwijk, Holland), ONSA (Onsala, Sweden), and WTZ1 (Wettzell, Germany) of Eurasia, TIDB (Tidbinbilla) of Australia, MASP (Mas Palomas, Canary Islands) of Africa, and OHIG (O'Higgins) of Antarctica. The a priori uncertainties were assigned values of 2, 2, and 4 mm/yr for their east, north, and up velocity components, respectively. The site velocity components at ONSA were constrained to be 1, 1, and 2 mm/yr to establish a velocity reference point. Very often space geodetic studies tie their results to a global geodetic velocity reference frame such as the ITRF94 [*Boucher*, 1996]. We did not take such an approach because our data set has included enough global stations to define a global frame by itself. Using the NNR NUVEL-1A model constraints also enables us to eliminate the free rigid body rotation inherently associated with a geodetic reference frame (see *Zhang et al.* [1999] for an assessment of the problem associated with the ITRF96 reference frame) and to make direct comparison with the predictions of a global tectonic model.

3. Results

Velocity results from the QOCA modeling are listed in Tables 1 and 2 and shown in Figure 1. All the velocities in Figure 1 are residual velocities of the NNR NUVEL-1A model, i.e., the velocity at Bangalore is referenced to the NNR NUVEL-1A India plate prediction, and all the rest are referenced to the NNR NUVEL-1A predictions of a stable Eurasia plate. The error ellipses show a ratio of ~1.2 between the east and north velocity components, different from the result of a typical GPS data analysis which usually demonstrates such a ratio as 1.5-2.0. We believe that the difference comes from the configuration of our regional network. Most of the regional fiducial stations are located east and west of the north China network, and the network itself is also in an east-west stripe. Such a configuration enhances the solution more for the east component than for the north and reduces the uncertainties accordingly. Figure 2 shows model predicted and observed time series at selected sites, including all the permanent sites in east Asia and all the survey mode sites in north China except those absent in the 1992 survey. The velocities are referenced to the NNR NUVEL-1A. All the observed time series show reasonable fit to a linear velocity, plus an antenna phase center jump after 1992 at the north China sites, indicating that the data are consistent with the fitting model. The antenna phase center jump from the Ashtech L12 to Z12 is resolved at -16±7, -19 ±7, and 45±90 mm for the east, north, and up components, respectively. These numbers are consistent within errors with our unpublished result derived from analyzing a different data set also collected in China with the same kind of receiver/antenna mixing. Such consistency gives us confidence that we are not artificially adding biased parameters.

The following characteristics of large-scale deformation in east Asia are derived from our solution:

1. The north China region is moving at ~5-11 mm/yr eastward relative to stable Eurasia (Figure 1). The deformation pattern reaches as far to the east as the Korea Peninsular where the station Taejon (TAEJ) shows a motion similar to that of the north China sites. The result is derived from data spanning up to 4 years and is accurate to ~2 mm/yr. The solution is not sufficient to differentiate velocity variations between individual stations. However, our result is sufficient to detect systematic variations between regions. We find that the stations located east of the

Table 2. East Asia Permanent Stations and Their Velocities

Site	Agency	Location	Longitude East			Latitude North			East, mm/yr NNRA	East, mm/yr GPS	East, mm/yr GPS-NNRA	East, mm/yr σ	North, mm/yr NNRA	North, mm/yr GPS	North, mm/yr GPS-NNRA	North, mm/yr σ	Corr	Occupation Year in 1900
CHAN	CSB	Changchun, China	125°	27'		43°	47'		20.3	25.2	4.9	1.4	-13.7	-12.6	1.1	1.1	-0.02	95,96
HAIK	CSB	Haikou, China	110°	20'		20°	0'		22.7	34.0	11.3	5.0	-11.0	-15.2	-4.2	2.0	-0.01	96,97
IISC	IGS	Bangalore, India	77°	34'		13°	1'		39.7	40.9	1.2	1.6	41.1	35.0	-6.1	1.3	-0.05	95-99
IRKT	IGS	Irkutsk, Russia	104°	19'		52°	13'		22.4	24.8	2.4	1.1	-9.7	-10.6	-0.9	1.0	-0.01	95-99
KIT3	IGS	Kitab, Uzbekistan	66°	53'		39°	8'		25.6	29.6	4.0	1.0	0.2	4.2	4.0	0.9	-0.01	95-99
LHAS	IGS	Lhasa, Tibet	91°	6'		29°	39'		24.6	44.9	20.3	1.3	-6.5	14.7	21.2	1.1	-0.03	95-99
POL2	IGS	Poligan, Kyrgyzstan	74°	42'		42°	41'		25.5	28.9	3.4	1.1	-2.0	3.6	5.6	1.0	-0.01	95-99
SHAO	IGS	Shanghai, China	121°	12'		31°	6'		21.9	31.1	9.2	1.3	-13.1	-15.8	-2.7	1.2	-0.02	95-99
TAEJ	IGS	Taejon, South Korea	127°	22'		36°	22'		20.8	26.8	6.0	1.5	-14.0	-18.3	-4.3	1.2	-0.02	96-98
TAIW	IGS	Taipei, Taiwan	121°	32'		25°	1'		22.0	31.9	9.9	1.4	-13.1	-14.0	-0.9	1.2	-0.02	95-99
TIAN	CSB	Tianjin, China	117°	16'		39°	6'		22.0	23.9	1.9	1.3	-12.4	-13.1	-0.7	1.2	-0.02	92,95-97
TSKB	IGS	Tsukuba, Japan	140°	5'		36°	6'		18.9	-7.7	-26.6	1.2	-15.5	-12.1	3.4	1.1	-0.02	95-99
URUM	CSB	Urumqi, China	87°	34'		43°	45'		24.8	31.7	6.9	1.4	-5.5	-0.3	5.2	1.1	-0.01	95,96,97
USU3	IGS	Usuda, Japan	138°	22'		36°	8'		19.1	-2.8	-21.9	1.2	-15.3	-9.6	5.7	1.1	-0.02	95-99
WUHN	IGS	Wuhan, China	114°	21'		30°	32'		22.7	32.1	9.4	1.3	-11.8	-14.4	-2.6	1.2	-0.02	96-99
XIAN	IGS	Xi'an, China	109°	13'		34°	22'		23.2	32.1	8.9	1.3	-10.8	-13.2	-2.4	1.1	-0.02	96-99

Entries are defined as in Table 1.

Shanxi Rift and south of a ESE-WNW trending seismic zone around 40°N latitude move at about 4±2 mm/yr east to ESE relative to the ones located west of the rift (Figures 3 and 4). Also, stations located east of the Shanxi Rift and south of the seismic zone mentioned above are moving on average about 1.8±1.0 mm/yr east-southeastward relative to their northern neighbors (Figures 3 and 4). The data are sparse across the Shandong section of the Tanlu Fault. Nevertheless, the differential velocity across the fault is probably no more than 3 mm/yr in both the along-strike and normal directions.

2. Southern China is moving east-southeastward, as at stations located in Shanghai (SHAO), Xi'an (XIAN), Wuhan (WUHN), and Haikou (HAIK). Our estimation shows that these stations move 9.5±1.3, 9.1±1.3, 9.7±1.3, and 12.1±4.0 mm/yr, in the directions of N106.5°±7.1°E, N104.7°±7.1°E, N104.9°±7.1°E, and N110.4°±15.0°E relative to the stable Eurasia plate, respectively.

3. Bangalore, India (IISC) is moving 41.9±1.4 mm/yr toward the Eurasian plate, at azimuth N25.5°±1.5°E. Such a relative motion is about 6.2±1.3 mm/yr, N169°±12°E different from the NUVEL-1A model prediction. This discrepancy is significant at the 95% confidence level.

4. Station LHAS in Lhasa, Tibet, is moving 29.4±1.2 mm/yr, N43.8°±2.4°E with respect to the stable Eurasia plate.

5. Three stations located from west to east along the north rim of the Tian Shan at Poligan (POL2), Kitab (KIT3), and Urumqi (URUM), respectively (Figure 1), display ~7-9 mm/yr northeast motion relative to the stable Eurasia plate. This velocity is significant at the 95% confidence level.

6. Close to the subduction zones, two Japanese sites TSKB (Tskuba) and USU3 (Usuda) show motion of 26.8±1.2 mm/yr, N83°±3°W and 22.6±1.2 mm/yr, N75°±3°W relative to the stable Eurasia plate, respectively. Station TAIW (Taipei, Taiwan) moves 9.9±1.4 mm/yr, N85°±8°E with respect to the stable Eurasia plate.

4. Discussion and Interpretations

4.1. Potential Bias of the Result Caused by Uncertainties of the Reference Frame

In our data modeling, we constrained station velocities at nine selected global tracking sites to their NNR NUVEL-1A values with uncertainties of 2, 2, and 4 mm/yr for the east, north, and up components, respectively. The velocity postfit residuals at the nine sites are all within their a priori uncertainties. However, will this approach bias our result? For example, is our solution in east Asia reliably tied to the "stable" Eurasia plate or could a rigid body rotation exist between the two? To answer this question, we performed a test of error propagation from the NUVEL-1A model to our solution. We first evaluated the station velocity uncertainties at our fiducial sites, propagated from the covariances of NUVEL-1 plate motion model [*DeMets et al.*, 1990, Table 5]. The horizontal uncertainties for those selected fiducial sites turned out to be ~1.3-2.0 mm/yr, assuming a fixed Pacific plate. Next, we reran our station velocity modeling using the velocity uncertainties of NUVEL-1 to constrain the fiducial station velocities. We found no significant differences in results of the two approaches. All the horizontal station velocity differences in Asia were < 1 mm/yr. The station velocity uncertainties are also comparable for the two approaches after the solution uncertainty rescaling as described above. We conclude that if the uncertainties of relative plate motions are properly accounted for in the NUVEL-1A model and the fiducial sites we selected justly

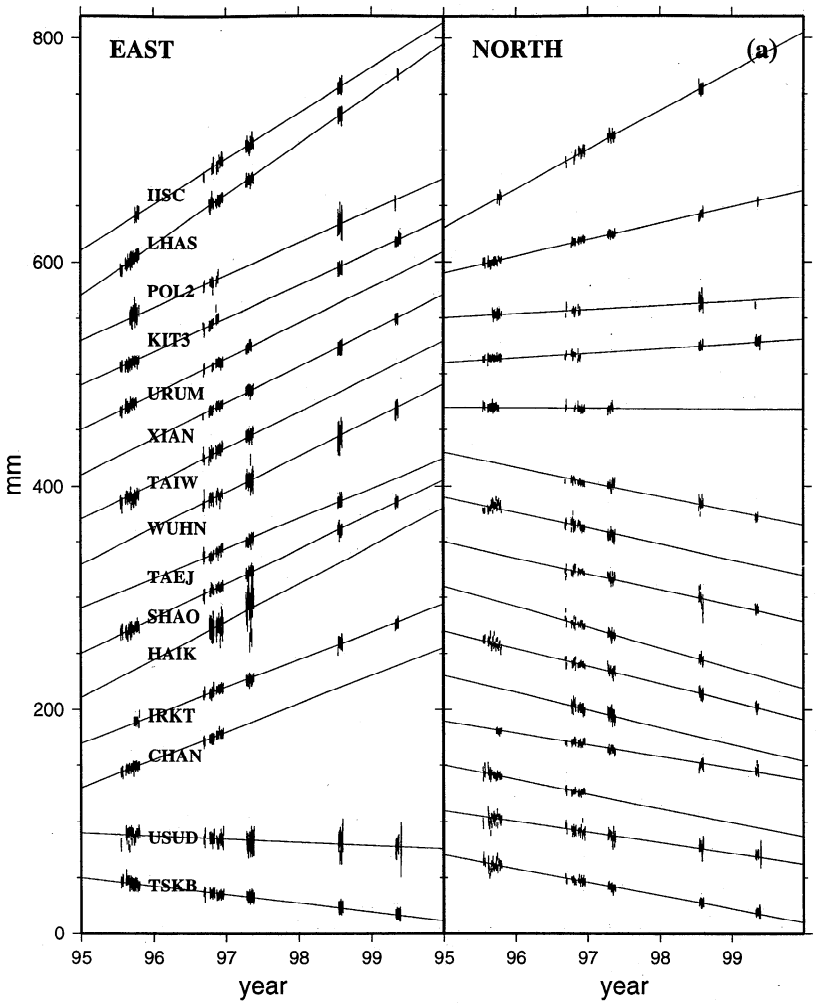

Figure 2. Time series of horizontal components of station positions. Data are shown with 1σ standard deviation. The solid lines are postfit model predictions. (a) East Asia permanent sites and (b) and (c) all the north China campaign mode sites first surveyed in 1992. The kinks in the prediction curves represent jumps induced by receiver/antenna changes.

represent the motion of the plates they reside on (the latter has been supported by previous studies such as *Larson et al.*, [1997]), our result should have no significant rotational bias and the station velocity uncertainties should be reasonable representations of the errors.

4.2. Tectonic Deformation in the North China Region

We have detected 4±2 mm/yr extension in the N105°E direction across the northern segment of the NNE-SSW trending Shanxi Rift. The extension zone to the east seems to include the range front faults, such as the Kouquan Fault, bounding the west edge of the rift. To the west, however, the extent of the extension zone is not well constrained, as the station coverage is sparse. The extension zone could include the eastern end of the Hetao Rift and a region between the Hetao Rift and the northern part of the Shanxi Rift (Figure 3).

Geological and geomorphologic studies revealed that the Shanxi Rift is composed of a cluster of S-shaped transtensional structures. At the southern end of the rift chain, Weihe Basin is located southwest of the Ordos plateau and strikes east-west. Farther north, Linfen, Taiyan, and Xinxian Basins are situated east of the plateau and strike NNE. At the northern end of the chain, Datong Basin is at the northeast corner of the plateau and strikes ENE [*Xu and Ma*, 1992; *Zhang et al.*, 1998]. Geomorphological studies revealed that the basins extended in the ESE direction and sheared dextrally along the faults bounding the basins, resulting in a regional strain of northeast compression and southeast extension [*Zhang et al.*, 1995, 1998]. The opening of the basins that we find agrees with the geological findings. However, our estimated extension direction is ~45° counterclockwise from the geological prediction.

What causes such a discrepancy? One possibility is that the geological findings revealed only part of the tectonic deformation in the region. The basins of the Shanxi Rift have been subsiding rapidly in Quaternary time. Although attempts have been made to determine fault slip rates using geomorphic and geodetic methods, estimates usually suffer from large uncertainties [*SSBRG*, 1988, Chapter 4; *Zhang et al.*, 1998]. This difficulty is compounded by the possibility that the extension may not be confined on the active faults bounding the basins. The basins are composed of thick unconsolidated sediments, and deformation may be spread over a broad region, as evidenced by the discovery of extensional fissures in the basins [*SSBRG*, 1988]. The geo-

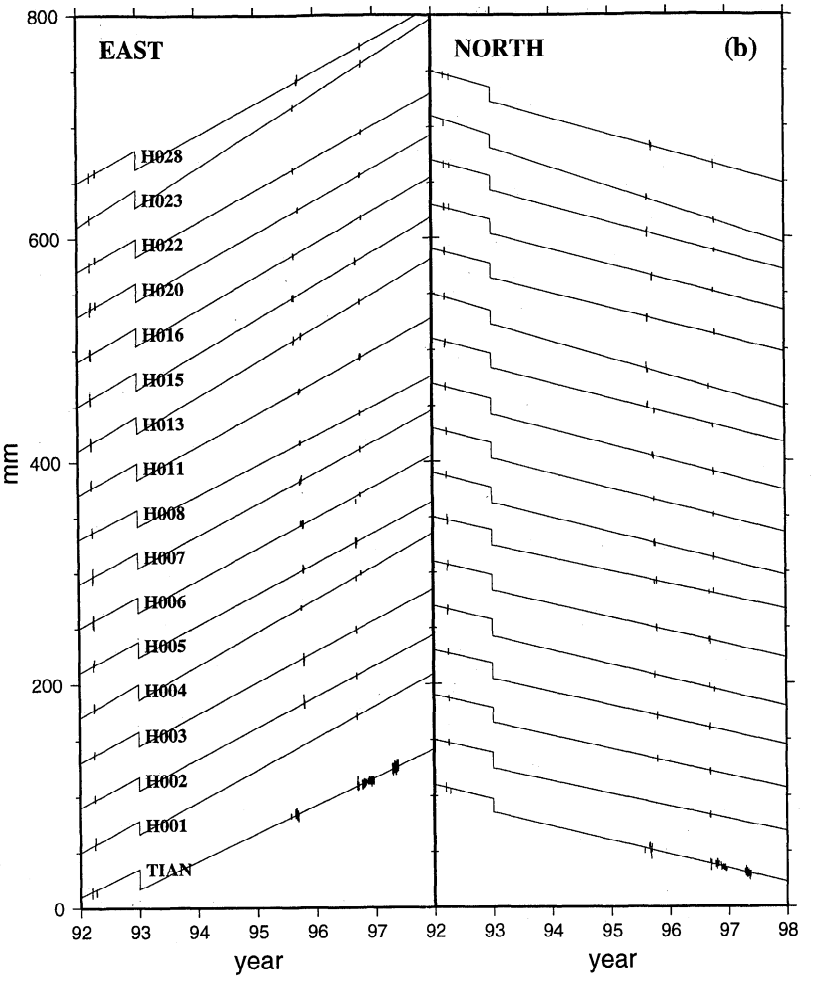

Figure 2. (continued)

logical and geomorphologic investigations, focused on the basin edge normal faults, may have found only a fraction of the horizontal extension, leading to underestimation of the east to ESE opening of the basins. For example, only 0.5 mm/yr extension was discovered across the central Shanxi Rift [*Zhang et al.*, 1998], much smaller than what we observe here.

Another possibility is that the opening rate may increase along the Shanxi Rift from south to north, and what we observe is the maximum opening at the northeast junction between the Shanxi and Hetao Rifts. Geological studies revealed that a young rift is being developed at the Daihai Basin east of the Hetao Rift [*SSBRG*, 1988, Chapter 3] (Figure 3). The basin is bounded by active tensional and transtensional faults. Three groups of faults trending NNE, ENE, and northwest coexist, and 0.2-0.4 mm/yr vertical displacement rates were estimated at some of the faults. The region is also seismically active. An earthquake of M 6.2 occurred along the Feicaizhuang-Qianyaozi Fault on April 6, 1976, and a number of M 5 events were recorded in the region for the last 3 decades (earthquake catalog from Z. Ding, China Seismological Bureau). In fact, this has been the most seismically active region in the vicinity for the last 3 decades, more active than the Datong Basin located to its southeast. West of the Daihai Basin, the Helinger Fault bounding the east end of the Hetao Rift may also contribute to the east-west extension. The fault was characterized as transtensional [*SSBRG*, 1988, Chapter 3], and is seismically active (Figure 3).

If the region is extending at a rate of 4 mm/yr in the ESE-WNW direction, what is its dynamic setting, and how is it related to the overall tectonics in east Asia? *Peltzer and Tapponnier* [1988], using mechanical simulation of indentation on plasticine models, demonstrated that eastward extrusion of the Tibetan block would cause extension in a region northeast of the Tibetan block where the Shanxi Rift is located. *Ye et al.* [1987] examined the rifting process of the north China platform, and proposed that north China was dominated by the rifting due to the Pacific-Eurasia collision in the east and by northeast extrusion of the Tibetan Plateau in the west, with the Taihang mountains (located east of the Shanxi Rift) as the boundary. Their conclusion is supported by *Northrup et al.* [1995], who found that during Tertiary time, rifting along the eastern plate margin was more prevalent when the relative plate motion was slower. Bouguer gravity [*Xu and Ma*, 1992] and seismic refraction [*Sun et al.*, 1988; *Zhang et al.*, 1988] studies revealed a 2-6 km uplift of the Moho depth beneath the Shanxi Rift. Average heat flow along the rift is 21% higher than the mean continental heat flow [*Wu et al.*, 1988], suggesting hot material upwelling from the upper mantle. Those geophysical observations, together with our geodetic results, suggest the existence of a deep rift system cutting through the entire lithosphere.

We consider three possible mechanisms for the opening of the Shanxi Rift. (1) The rift system could have been produced by the differential eastward motion between the Tibetan Plateau and

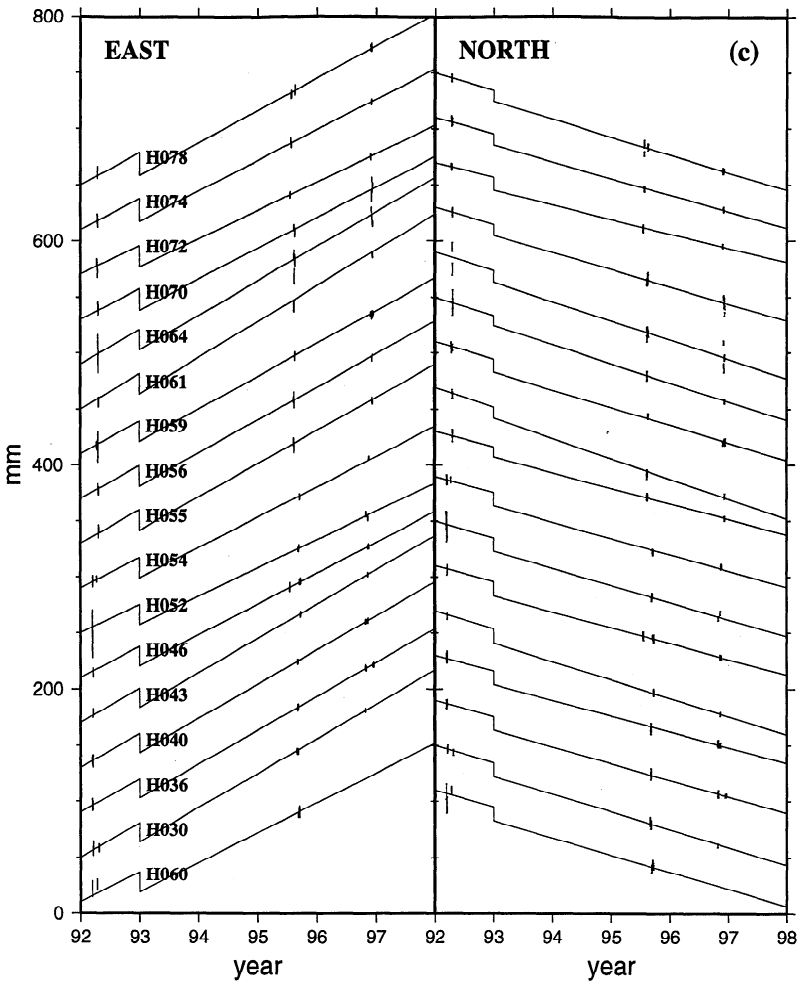

Figure 2. (continued)

north China, creating extensional basins as suggested by *Peltzer and Tapponnier* [1988], *Ye et al.* [1987], and *Xu and Ma* [1992]. (2) It could also be possible that the counterclockwise rotation of the Ordos block, initiated by the eastward extrusion of the Tibetan Plateau imposed southeast of the block, has created extensional deformation around the northeast corner of the block. If so, it should also cause right-lateral transtensional motion (with less extensional but more shear than the northern part) along the central and southern part of the Shanxi Rift from the Xinxian Basin to the Lifen Basin. (3) The extension could have been produced as part of the backarc spreading process for the Pacific and Philippine Sea plates subducting beneath the Eurasian continent [*Northrup et al.*, 1995]. Probably all three mechanisms have played roles in the rift creation and extension, but how much has been contributed by each of the three processes during the time of the rift development is still subject to investigation. It is certain, though, that more geodetic measurements in the region are needed to differentiate deformation patterns produced by the three possible mechanisms.

Another deformation pattern in the region is that east of the Shanxi Rift, the southern stations move slightly faster to the east than the northern stations (Figure 3). This pattern can be interpreted in two ways. One is to describe the deformation by a rigid rotation of a single block, and the other is to allow translation between the southern and northern networks. An inversion of the geodetic velocities of the stations located east of the Shanxi Rift in the north China region yields an estimation of the block rotation with respect to stable Eurasia of 3.9±1.1 nrad/yr, with the rotation pole located at 61°N latitude and 120°E longitude. The second model, allowing translation between two subnetworks separated by the seismic zone around the 39.7°N latitude, gives 1.8±1.0 east-southeastward motion of the north China plain relative to the Mongolia region. The 40°N seismic zone crosses the Datong Basin and defines the Yan Shan-north China plain boundary. Part of the zone is delineated by the Nankou-Sunhe Fault to the south (Figure 3). Geological studies confirmed that this is an active left-lateral strike-slip fault [*Ma*, 1987], consistent with our interpretation here. The translation model is marginally better than the rotation model, as the former is favored at 66% confidence in an F test. The result suggests an east-southeastward sliding of the north China plain caused probably by eastward push from its southern neighbor or by the rifting process of the Shanxi Rift. If the Shanxi Rift were to mimic an oceanic spreading ridge, the north rim deformation zone of the north China plain would then serve as a transform fault.

It is ironic to find that the reference station for the north China network at Tianjin (TIAN) shows anomalous motion relative to the other sites in the region. We believe that the anomaly is caused by monument instability. While most of the campaign mode sites are bedrock sites, TIAN is located about 25 m above the ground surface at the top of a seven-story building, the headquarters of the FCDMC. The building is on sediments and could

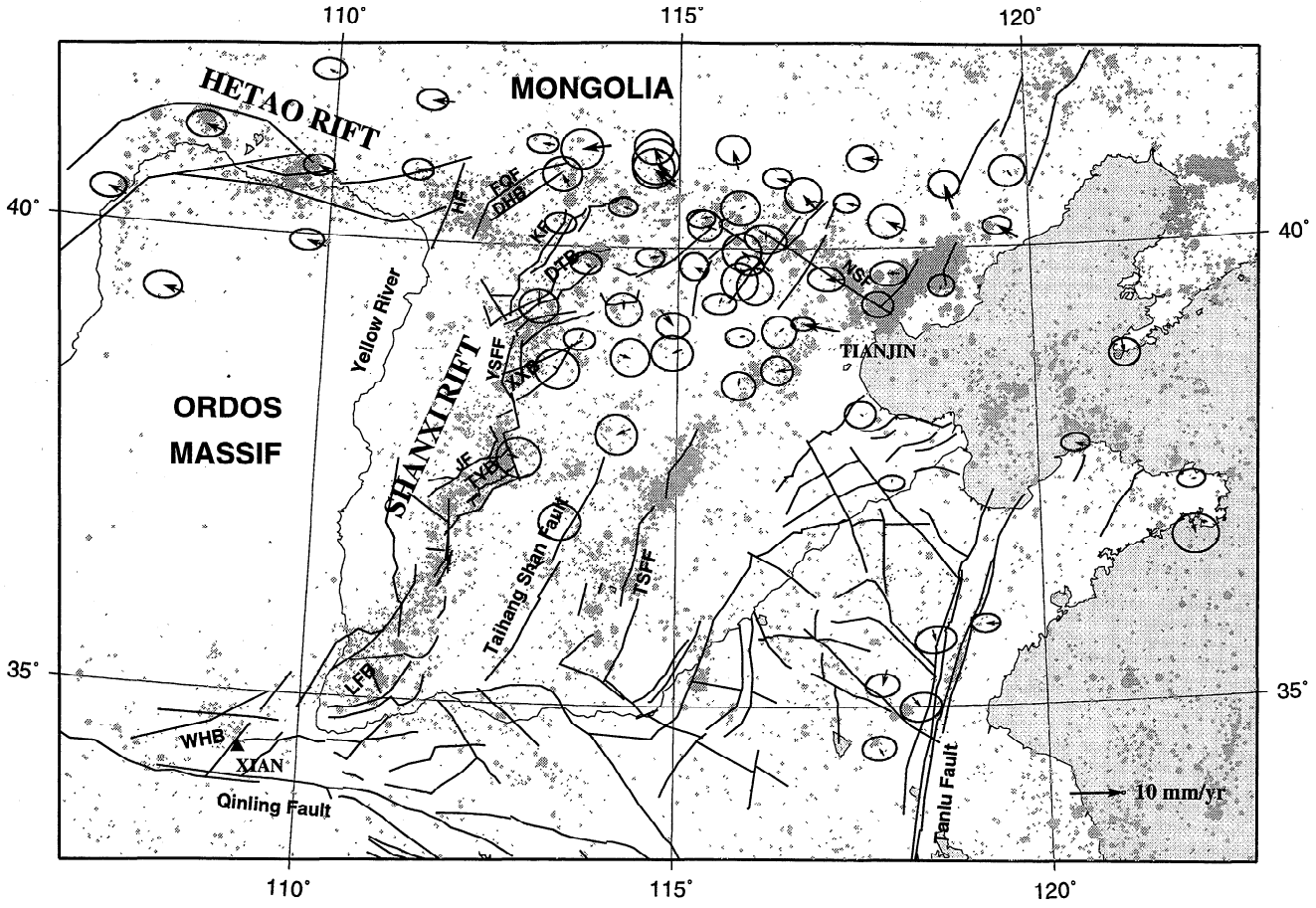

Figure 3. Close-up view of station residual velocities in north China with respect to XIAN. The error ellipses represent 95% confidence. Thick lines are faults, and thin lines are the rivers. The shaded dots represent earthquake epicenters whose sizes are proportional to the magnitudes. Abbreviations are: WHB, Weihe Basin; LFB, Linfeng Basin; TYB, Taiyuan Basin; XXB, Xinxian Basin; DTB, Datong Basin; DHB, Daihai Basin; TSFF, Taihang Shan Frontal Fault; JF, Jiaocheng Fault; YSFF, Yunzhong Shan Frontal Fault; KF, Kouquan Fault; FQF, Feicaizhuang-Qianyaozi Fault; HF, Helinger Fault; NSF, Nankou-Sunhe Fault.

have been tilting slowly westward. We do not think the instability of the reference site would seriously compromise our GPS velocity estimates, because its local motion seems to be steady. In the crustal deformation analyses mentioned above we have excluded the site.

It has been recognized that two sets of conjugate faults exist in the central section of the Tanlu Fault system, with the primary set oriented NNE and showing right-lateral motion and the secondary set oriented northwest and showing left-lateral motion [*Ma*, 1987]. There is also a strong thrust component for both sets of the faults [*Wei et al.*, 1993, Chapter 7]. We found that the differential velocity across the fault is insignificant at the error level of ~2 mm/yr, indicating that the slip rate along the fault is probably no more than 3 mm/yr.

4.3. Tectonic Motion in East, Central, and South China

We observe SHAO (Shanghai) moving 9.5±1.3 mm/yr in the direction of N107°±7°E. This observation agrees well with the Very Long Baseline Interferometry (VLBI) estimate, 11 mm/yr, N112°E at the site [*Heki*, 1996]. Station velocities at another two central China sites, XIAN (Xi'an) and WUHN (Wuhan) are similar to that at Shanghai, suggesting that southeastern China moves ~10 mm/yr east-southeastward with respect to the stable Eurasia. This result is generally consistent with the ~12 mm/yr eastward motion of the same stations estimated by *Burchfiel et al.* [1998]. Our data lack the spatial resolution to constrain slip rates on specific faults. Nevertheless, the deformation pattern seems to be consistent with *Houseman and England*'s [1993] estimate of the south China eastward motion rate which yields about ¼ of the ~50 mm/yr indentation rate at the Indo-Asia plate boundary. Our result is also marginally consistent with *Avouac and Tapponnier*'s [1993] minimum estimate of the southeastward motion of south China, given as ~10-15 mm/yr.

Station XIAN seems to move along with the north and central China sites west of the Shanxi Rift, which move about 4±2 mm/yr faster to the east than the sites on the northern part of the Ordos block. *Zhang et al.* [1998] estimated 5±2 mm/yr left-lateral motion between Mongolia and the Weihe Basin where station XIAN is located, caused by the counterclockwise rotation of the Ordos block. They also determined another 7±2 mm/yr left-lateral motion between the Weihe Basin and south China across the Qinling Fault zone (Figure 3). Assuming XIAN is on the Ordos block, our result of 4 mm/yr eastward motion at XIAN with respect to the northern Ordos block is compatible to Zhang et al.'s 5±2 mm/yr estimate. However, we find virtually no relative motion between XIAN and WUHN, which is located ~600 km southeast of XIAN. *Zhang et al.*'s [1998] estimate of 7±2 mm/yr relative motion along the Qinling Fault Zone, if true, must

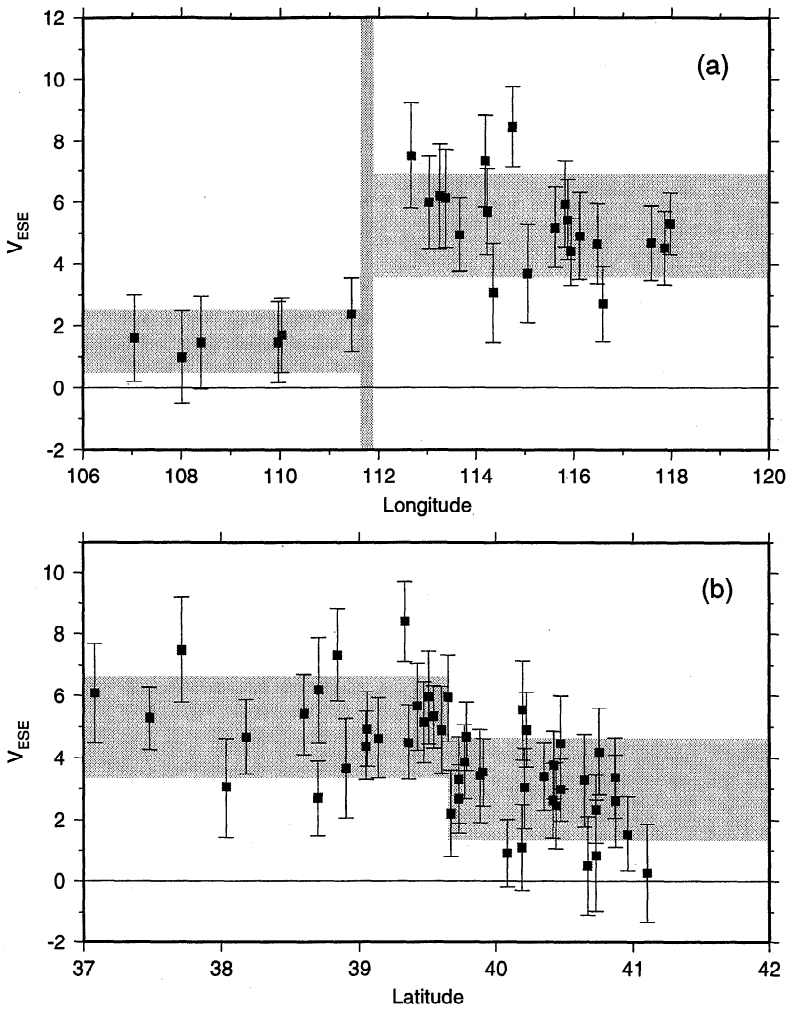

Figure 4. Velocity profiles across the Shanxi Rift zone and the 40°N seismic zone. All the station velocities are referenced to XIAN and projected to the N105°E direction. (a) Velocity profile across the Shanxi Rift zone. Sites included east of the rift zone are those located west of 119°E longitude and between 37°N and 39.6°N longitude. Sites included west of the rift zone are those located inside and south of the Hetao Rift. A vertical line marks the approximate location of the Shanxi Rift. Light shaded areas are the approximate data spans on both sides of the rift zone. A 4±2 mm/yr extension is detected across the rift zone. (b) Velocity profile across the 40°N seismic zone. Sites included are those located north of 36°N latitude and between the Shanxi Rift zone and 120°E longitude. The light shaded areas are the approximate data spans across the seismic zone. Notice the left lateral-shear pattern centered at ~39.7°N longitude. The shear motion rate between two groups of sites separated at this latitude is 1.8±1.0 mm/yr.

be within a localized region, because it is not detected 600 km away from the fault zone. However, such a deformation pattern would require strain concentration east and south of the Qinling Fault zone, which has not been observed geologically.

Along the east margin of the Tibetan Plateau, geological studies placed ~13 mm/yr left-lateral strike-slip motion along the Kunlun Fault [*Van der Woerd et al.*, 1998] and ~15 mm/yr left-lateral motion along the Xianshuihe Fault [*Allen et al.*, 1991]. *King et al.* [1997] (see also *Burchfiel et al.*, [1998] for their recent result) analyzed GPS data observed at the eastern boundary of the Tibetan Plateau and found 12±4 mm/yr left-lateral motion along the Xianshuihe-Xiaojiang Fault system. *King et al.*'s [1997] result also suggested no east-west shortening across these faults. However, it is inconclusive whether the whole region might have been extruded eastward. Our result yields about 24±2 mm/yr right-lateral motion along the strike of the Xiaojiang Fault between Lhasa and Wuhan. Because this rate is in opposite direction to the actual sense of geological slip along the Xiaojiang Fault, between Lhasa and Wuhan there is a total of 36 mm/yr right-lateral motion unaccounted for. It is possible that such a required right-lateral motion is accommodated through clockwise rotation of the eastern Tibet block [e.g., *England and Molnar*, 1990; *Royden et al.*, 1997]. More data, however, are required to pin down the spatial rotation pattern west of the Xianshuhe-Xiaojiang Fault system. About 11±2 mm/yr east-west shortening is detected between Lhasa and Wuhan. The shortening between LHAS and SHAO is 11.2 mm/yr, which is consistent with a rate of 9.6 mm/yr we estimate from Table 2 of *Larson et al.* [1999]. (*Larson et al.* [1999] claimed no shortening between LHAS and SHAO. Their conclusion was based on a comparison of the station velocities at LHAS and SHAO. It seems that part of the station velocity at LHAS parallel to the Indo-Asian relative plate motion was not accounted for in their comparison.) This shortening, if not taking place across the Xianshuihe-Xiaojiang Fault

system, would have to be accommodated somewhere else along the eastern margin of the Tibetan Plateau, again possibly related to the clockwise rotation of the eastern Tibet block.

The 12±4 mm/yr southeast motion of station HAIK in south China suggests a similar motion pattern to the north and east China, with a slight increase in magnitude. This is somewhat uncertain, however, because of the large uncertainty of the velocity estimate. Nevertheless, our observed southeast motion of the site suggests that the Hainan Island region moves coherently with the south China block.

4.4. Indo-Eurasian Relative Plate Motion

If the velocity at Bangalore represents rigid motion of the India plate, its 41.9±1.4 mm/yr, N25.5°±1.5°E motion toward the Eurasia plate suggests that the India plate is moving ~6 mm/yr slower toward Himalaya than NUVEL-1A predicted. Whether the discrepancy is due to a recent change in plate motion rate (timescale of a few years) from its previous 2 Myr average or due to other reasons remains to be seen. The site is on bedrock and should be stable (R. Bilham, personal communication, 1999). Previous studies by *Freymueller et al.* [1996] and *Larson et al.* [1999] differ from the NUVEL-1A by 4±5 mm/yr, S34°W and 3±2 mm/yr, S50°W, respectively. Our result is 4.5±2.0 mm/yr, S13°W from Larson et al.'s. The difference is not small but still not significant at 95% confidence. The cause of the discrepancy is not clear. Both Larson et al. and Freymueller et al. used earlier GPS data at the site, with the 1991 and 1994-1997 measurements made at different local monuments and being tied together later. The tie made between the two local sites in their studies might be a concern, and the difference in time span of the data (theirs 1991 and 1994-1997 versus ours 1995-1999) could also be a factor. It is also possible that different constraints on the reference frame in GPS data modeling might induce some systematic differences.

4.5. Convergence Rate at the Himalaya Plate Boundary

Assuming that the plate interiors are rigid from Bangalore to the southern Himalaya in India and from the northern Himalaya to Lhasa in Asia, we can infer the convergence rate based on the relative velocity of IISC with respect to LHAS. It requires 3 degrees of freedom to define a rigid body rotation around a vertical pole. However, a single station velocity offers only 2. To solve this underdetermined problem, we assume that the station velocity at IISC coincides with the India plate motion, and that the NUVEL-1A model correctly predicts the relative plate motion direction. The convergence rate at the plate boundary is then estimated at 22.0±2 mm/yr. Our result also agrees with the 18±2 mm/yr convergence across the Himalaya estimated by *Bilham et al.* [1997] and *Larson et al.* [1999] using GPS data. Their data were collected from a network ~200 km wide across the mountain range, so the difference between our estimate and theirs could be explained by residual deformation beyond their network coverage. Our Eurasia fixed station velocity of 29.4±1.2 mm/yr, N43.8°±2.4°E at LHAS agrees with *Larson et al.*'s [1999] estimate of 30±3 mm/yr, N40°±4°E. It also agrees with *Kato et al.*'s [1998] amplitude estimate of 31±3 mm/yr but differs somewhat from their direction estimate of N53°±3°E. The component of LHAS velocity perpendicular to the India-Eurasia relative motion direction (N15°±3°E at the site) is 14.2±1.3 mm/yr. This motion may have either been related to eastward extrusion of the relatively rigid Tibetan Plateau [*Armijo et al.*, 1986] or distributed east-west extension of a less rigid Tibetan block [*Larson et al.*, 1999; *Yin et al.*, 1999]. Such a partition of the station velocity at LHAS depends on the Indo-Asia relative motion direction defined by NUVEL-1A. As discussed above, the NUVEL-1A result for this estimation is under question. If, say, the plate relative motion direction were N20°E instead of N15°E, the velocity component normal to the relative plate motion direction at LHAS would be 12.3 mm/yr instead of 14.2 mm/yr as given above. However, if one cares only how much LHAS has moved eastward with respect to the stable Eurasia plate (resulting from Indo-Asia collision), our result yields an estimate of 20.3±1.3 mm/yr. This is a robust estimate because it depends only on the ties of our global network to a number of plates which are well defined in NUVEL-1A and is independent of the less known Indo-Asian relative plate motion.

4.6. Tectonic Deformations North of the Tian Shan

The three permanent stations located along the north rim of the Tian Shan show ~7-9 mm/yr northeast motion with respect to stable Eurasia, and the motion is statistically significant. The results are in good agreement with that of *Larson et al.* [1999]: 5.5±1.0 mm/yr toward N45°E versus 3.5±2 mm/yr toward N47°E at KIT3 and 6.6±1.0 mm/yr toward N31°E versus 6.5±3 mm/yr toward N29°E at POL2, respectively. (Larson et al. did not estimate the velocity at URUM.) As we discussed earlier, a rigid body rotation error of central Asia about Europe caused by the uncertainties in the NUVEL-1A model cannot be significant enough to explain this deformation. A more likely explanation, we think, is that there is still remnant deformation in the region north of the three stations. The region north of the three sites is seismically active, as evidenced by the occurrences of medium to large sized (up to magnitude 8) earthquakes in the region during the past several decades [*Institute of Geophysics*, 1976] (also, for earthquakes since 1976, http://www.seismology.harvard.edu/CMTsearch.html). Geologically, a number of dextral strike-slip faults, such as the Talasso-Fergana Fault and the Junggar Fault, may have accommodated this motion [*Tapponnier and Molnar*, 1979, Figure 1]. Active blind thrust ramps may exist beyond the north rim of the Tian Shan. One such ramp was found 30 km north of the Tian Shan range, northwest of Urumqi [*Avouac et al.*, 1993]. *Ma* [1987] showed similar active structures east of Avouac et al.'s study area. The 7 mm/yr north component of station URUM must include a 3 mm/yr north-south convergence discovered along this thrust system in the northern most Tian Shan. In addition, ~5-7 mm/yr differential motion exists between the three central Asia sites and station IRKT at Irkutsk, mainly in the north direction. This might be explained by the dextral shear motion in the Altai Fault system between them. Although no precise measurements of near-field deformation are available, the Altai Fault system is known to be tectonically active, as evidenced by the occurrence of large earthquakes (four $M \sim 8$ events occurred there this century [*Baljinnyam et al.*, 1993]).

Acknowledgments. We thank many organizations and individuals who have provided data to this project, particularly those responsible for the establishment and maintenance of the sites in Asia: Vjacheslav Zalutsky (IRKT), Shuhrat Ehgamberdiev (KIT3), Jing-Nan Liu (WUHN), An-Xin Ma (XIAN), Wenyao Zhu (SHAO), Chong Cao (HAIK), Yanping Zhang (URUM), Pil-Ho Park (TAEJ), Chi-Ching Liu (TAIW), Mitsuo Yamada (USU3), R. N. Singh (IISC), IGS Group of GIS, Japan (TSKB), Juergen Neumeyer, Wolfgang Schlueter, Bernd Richter, Ruth Neilan, and Gotou Katsuhiro. We also thank Yehuda Bock for providing the IGS data archive. Xinkang Hu assisted in the early processing of the north China data. Min Wang's assistance with the data processing during the

manuscript revision is especially appreciated. Comments by Tim Dixon, Roger Bilham, and Roland Burgmann helped improve the manuscript greatly. We are also grateful to Peter Molnar and Bob King for informative discussions and comments on the manuscript and to Zhifeng Ding for providing us a north China earthquake catalog. Several figures were plotted using the GMT software [*Wessel and Smith*, 1991]. This research was funded by NSF grants INT9602179, EAR9614877, and EAR9805010.

References

Abdrakhmatov, K., et al., Relatively recent construction of the Tien Shan inferred from GPS measurements of present-day crustal deformation rates, *Nature*, *384*(6608), 450-453, 1996.

Allen, C. R., Z. Lou, H. Qian, X. Wen, H. Zhou, and W. Huang, Field study of a highly active fault zone: the Xianshuihe fault of southwestern China, *Geol. Soc. Am. Bull.*, *103*, 1178-1199, 1991.

Argus, D. F., and R. G. Gordon, No-net-rotation model of current plate velocities incorporating plate motion model NUVEL-1, *Geophys. Res. Lett.*, *18*, 2039-2042, 1991.

Armijo, R., P. Tapponnier, J. L. Mercier, and Han T., Quaternary extension in southern Tibet: Field observations and tectonic implications, *J. Geophys. Res.*, *91*, 13,803-13,872, 1986.

Avouac, J. P., and Tapponnier, Kinematic model of active deformation in central Asia, *Geophys. Res. Lett.*, *20*, 895-898, 1993.

Avouac, J. P., P. Tapponnier, M. Bai, H. You, and G. Wang, Active thrusting and folding along the northern Tien Shan and Late Cenozoic rotation of the Tarim relative to Dzungaria and Kazakhstan, *J. Geophys. Res.*, *98*, 6755-6804, 1993.

Baljinnyam, I., A. Bayasgalan, B. A. Borisov, A. Cisternas, M. G. Dem'yanovich, L. Ganbaator, V. M. Kochetkov, R. A. Kurushin, P. Molnar, H. Philip, and Y. Y. Vashchilov, Ruptures of major earthquakes and active deformation in Mongolia and its surroundings, Mem. *Geol. Soc. Am.*, *181*, 62 pp., 1993.

Bendick, R., R. Bilham, G. Yin, K. Larson, G. Peltzer, and J. Freymueller, Slip rate of the Altyn Tagh fault at 90 degrees east, *Eos Trans. AGU*, *79*(45), Fall Meet. Suppl., F203, 1998.

Bilham, R., K. Larson, J. Freymueller, and Project Ldylhim Members, GPS measurements of present-day convergence across the Nepal Himalaya, *Nature*, *386*(6620), 61-64, 1997.

Blewitt, G., Y. Bock, and G. Gendt, Regional clusters and distributed processing, paper presented at the IGS Analysis Center Workshop, Int. GPS Serv., Ottawa, Oct. 12-14, 1993.

Boucher, C., Z. Altamimi, M. Feissel, and P. Sillard, Results and analysis of the ITRF 94, *IERS Tech. Note 20*, Int. Earth Rotation Serv., Cent. Bur., Obs. de Paris, Paris, 1996.

Burchfiel, B. C., Chen Z., Liu Y., and L. H. Royden, Tectonics of the Longmen Shan and adjacent regions, central China, *Int. Geol. Rev.*, *37*, 661-735, 1995.

Burchfiel, B. C., R. W. King, L. H. Royden, E. Wang, Z. Chen, X. Zhang, and J. Zhao, GPS results from the entire eastern part of the Tibetan plateau and its adjacent foreland and their tectonic interpretation, *Eos Trans. AGU*, *79*(45), Fall Meet. Suppl., F204, 1998.

DeMets, C., R. G. Gordon, D. F. Argus, and S. Stein, Current plate motions, *Geophys. J. Int.*, *101*, 425-478, 1990.

DeMets, C., R. G. Gordon, D. F. Argus, and S. Stein, Effect of recent revisions to the geomagnetic reversal time scale on estimates of current plate motions, *Geophys. Res. Lett.*, *21*, 2191-2194, 1994.

Dixon, T. H., An introduction to the Global Positioning System and some geological applications, *Rev. Geophys.*, *29*, 249-276, 1991.

Dong, D., T. A. Herring, and R. W. King, Estimating regional deformation from a combination of space and terrestrial geodetic data, *J. Geod.*, *72*, 200-214, 1998.

England, P., and P. Molnar, Right-lateral shear and rotation as the explanation for strike-slip faulting in eastern Tibet, *Nature*, *344*(6262),140-142, 1990.

England, P., and P. Molnar, The field of crustal velocity in Asia calculated from Quaternary rates of slip on faults, *Geophys. J. Int.*, *130*, 551-582, 1997.

England, P. C., and G. A. Houseman, The mechanics of the Tibetan Plateau, *Philos. Trans. R. Soc. London, Ser. A*, *326*(1589), 301-320, 1988.

Feigl, K. L., et al., Measurement of the velocity field of central and southern California, 1984-1992, *J. Geophys. Res.*, *98*, 21,677-21,712, 1993.

Freymueller, J., R. Bilham, R. Burgmann, K. M. Larson, J. Paul, S. Jade, and V. Gaur, Global positioning system measurements of Indian plate motion and convergence across the Lesser Himalaya, *Geophys. Res. Lett.*, *23*, 3107-3110, 1996.

Gaudemer, Y., P. Tapponnier, B. Meyer, G. Peltzer, Guo S., Chen Z., Dai H., and I. Cifuentes, Partitioning of crustal slip between linked active faults in the eastern Qilian Shan, and evidence for a major seismic gap, the 'Tianzu gap', on the western Haiyuan fault, Gansu (China), *Geophys. J. Int.*, *120*, 599-645, 1995.

Harrison, T. M., P. Copeland, W. S. F. Kidd, and A. Yin, Raising Tibet, *Science*, *255*, 1663-1670, 1992.

Heki, K., Horizontal and vertical crustal movements from three-dimensional very long baseline interferometry kinematic reference frame: Implication for the reversal timescale revision, *J. Geophys. Res.*, *101*, 3187-3198, 1996.

Herring, T. A., GLOBK: Global Kalman filter VLBI and GPS analysis program, version 4.0, Mass. Inst. of Technol., Cambridge, 1995.

Holt, W. E., M. Li, and A. J. Haines, Earthquake strain rates and instantaneous relative motions within central and eastern Asia, *Geophys. J. Int.*, *122*, 569-593, 1995.

Houseman, G. A., and P. C. England, Crustal thickening versus lateral expulsion in the India-Asian continental collision, *J. Geophys. Res.*, *98*, 12,233-12,249, 1993.

Institute of Geophysics, The catalog of strong shocks of China, Acad. Sin., Beijing, 1976.

Kato, T., et al., Initial results from WING, the continuous GPS network in the western Pacific area, *Geophys. Res. Lett*, *25*, 369-372, 1998.

Kidd, W. S. F., and P. Molnar, Quaternary and active faulting observed on the 1985 Academia Sinica-Royal Society geotraverse of Tibet, *Philos. Trans. R. Soc. London, Ser. A*, *327*, 337-363, 1988.

King, R. W., and Y. Bock, Documentation for the MIT GPS analysis software: GAMIT, version 9.3, Mass. Inst. of Technol., Cambridge, 1995.

King, R. W., F. Shen, B. C. Burchfiel, L. H. Royden, E. Wang, Z. Chen, Y. Liu, X.-Y. Zhang, J.-X. Zhao, and Y. Li, Geodetic measurement of crustal motion in southwest China, *Geology*, *25*, 179-182, 1997.

Kong, X., and P. Bird, Neotectonics of Asia: Thin-shell finite-element models with faults, in *Tectonic Evolution of Asia*, edited by A. Yin and T. M. Harrison, pp. 18-34, Cambridge Univ. Press, New York, 1996.

Larson, K. M., J. T. Freymueller, and S. Philipson, Global plate velocities from the Global Positioning System, *J. Geophys. Res.*, *102*, 9961-9981, 1997.

Larson, K. M., R. Burgmann, R. Bilham, and J. T. Freymueller, Kinematics of the India-Eurasia collision zone from GPS measurements, *J. Geophys. Res.*, *104*, 1077-1093, 1999.

Leloup, P. H., and J. Kienast, High-temperature metamorphism in a major strike-slip shear zone: The Ailao Shan-Red River, People's Republic of China, *Earth Planet. Sci. Lett.*, *118*, 213-234, 1993.

Ma, X., Explanatory notes for the lithospheric dynamics map of China and adjacent seas, Geol. Publ. House, Beijing, China, 1987.

Mao, A., C. G. A. Harrison, and T. H. Dixon, Noise in GPS coordinate time series, *J. Geophys. Res.*, *104*, 2797-2816, 1999.

Molnar, P., and P. Tapponnier, Cenozoic tectonics of Asia; effects of a continental collision, *Science*, *189*, 419-426, 1975.

Neilan, R., The evolution of the IGS global network, current status, and future aspects, in *IGS Annual Report*, edited by J. F. Zumberge et al., *JPL Publ. 95-18*, 25-34, 1995.

Northrup, C. J., L. H. Royden, and B. C. Burchfiel, Motion of the Pacific plate relative to Eurasia and its potential relation to Cenozoic extension along the eastern margin of Eurasia, *Geology*, *23*, 729-722, 1995.

Peltzer, G., and F. Saucier, Present-day kinematics of Asia derived from geologic fault rates, *J. Geophys. Res.*, *101*, 27,943-27,956, 1996.

Peltzer, G., and P. Tapponnier, Formation and evolution of strike-slip faults, rifts, and basins during the India-Asia collision: An experimental approach, *J. Geophys. Res.*, *93*, 15,085-15,117, 1988.

Peltzer, G., P. Tapponnier, and R. Armijo, Magnitude of late Quaternary left-lateral displacements along the north edge of Tibet, *Science*, *246*, 1285-1289, 1989.

Royden, L. H., B. C. Burchfiel, R. W. King, E. Wang, Z. Chen, F. Shen, and Y. Liu, Surface deformation and lower crustal flow in eastern Tibet, *Science*, *276*, 788-790, 1997.

Shen, Z.-K., D. Dong, T. Herring, K. Hudnut, D. Jackson, R. King, S. McClusky, and L. Sung, Geodetic measurements of southern California crustal deformation, *Eos, Trans. AGU*, *78*, 477, 482, 1997.

State Seismological Bureau Research Group (SSBRG), Active fault system around Ordos Massif (in Chinese), Seismol. Press, Beijing, China, 1988.

Sun, W. C., Zhu Z. P., Zhang L., Song Y. J., Zhang C. K., and Zhong Y. J., Exploration of the crust and upper mantle in north China (in Chinese), in *Development in the Research of Deep Structures of China's Continent*, pp. 19-37, Geol. Publ. House, Beijing, China, 1988.

Tapponnier, P., and P. Molnar, Active faulting and tectonics in China, *J. Geophys. Res.*, *82*, 2905-2930, 1977.

Tapponnier, P., and P. Molnar, Active faulting and Cenozoic tectonics of the Tien Shan, Mongolia, and Baykal regions, *J. Geophys. Res.*, *84*, 3425-3459, 1979.

Van der Woerd, J., F. J. Ryerson, P. Tapponnier, Y. Gaudemer, R. Finkel, A. S. Meriaux, M. Caffee, Zhao G., and He Q., Holocene left-slip rate determined by cosmogenic surface dating on the Xidatan segment of the Kunlun Fault (Qinghai, China), *Geology*, *26*, 695-698, 1998.

Wang, E., B. C. Burchfiel, L. H. Royden, Chen L., Chen J., Li W., and Chen Z., Late Cenozoic Xianshuihe-Xiaojiang, Red River, and Dali fault systems of southwestern Sichuan and central Yunnan, China, *Spec. Pap. Geol. Soc. Am.*, *327*, 108 pp., 1998.

Wei, G. X., Diao S. Z., and Zhou C. Y., Study of seismicity along the Tancheng-Lujiang seismic zone (in Chinese), Seismol. Press, Beijing, China, 1993.

Wessel, P., and W. H. F. Smith, Free software helps map and display data, *Eos Trans. AGU*, *72*, 441, 445-446, 1991.

Wu, Q. F., Xie Y. Z., Zu J. H., and Wang D., A study on the geothermal field in north China (in Chinese), *Earthquake Res. China*, *4*, 41-48, 1988.

Xu, X., and X. Ma, Geodynamics of the Shanxi rift system, China, *Tectonophysics*, *208*, 325-340, 1992.

Ye, H., Zhang B., and Mao F., The Cenozoic tectonic evolution of the great north China: Two types of rifting and crustal necking in the great north China and their tectonic implications, *Tectonophysics*, *133*, 217-227, 1987.

Yin, A., S. Nie, P. Craig, T. M. Harrison, X. Qian, and G. Yang, Late Cenozoic tectonic evolution of the southern Chinese Tian Shan, *Tectonics*, *17*, 1-27, 1998.

Yin, A., P. A. Kapp, M. A. Murphy, C. E. Manning, T. M. Harrison, M. Grove, Ding L., Deng X.-G., and Wu C.-M., Significant late Neogene east-west extension in northern Tibet, *Geology*, *27*, 787-790, 1999.

Zhang, J. Y. Bock, H. Johnson, P. Fang, S. Williams, J. Genrich, S. Wdowinski, and J. Behr, Southern California Permanent GPS Geodetic Array: Error analysis of daily position estimates and site velocities, *J. Geophys. Res.*, *102*, 18,035-18,055, 1997.

Zhang, Q., Zhu W., and Xiong Y., Global plate motion models incorporating the velocity field of ITRF96, *Geophys. Res. Lett.*, *26*, 2813-2816, 1999.

Zhang, S., Chen X., Ding Y., Zheng C., Wu L., and Zhao J., Interpretation of Menyuan-Pingliang-Weinan DSS profile in west China (in Chinese), in *Development in the Research of Deep Structures of China's Continent*, pp. 61-67, Geol. Publ. House, Beijing, China, 1988.

Zhang, Y. Q., P. Vergely, and J. L. Mercier, Active faulting in and along the Qinling Range (China) inferred from SPOT image and extrusion tectonics of south China, *Tectonophysics*, *243*, 69-95, 1995.

Zhang, Y. Q., J. L. Mercier, and P. Vergely, Extension in the graben system around the Ordos (China), and its contribution to the extrusion tectonics of south China with respect to Gobi-Mongolia, *Tectonophysics*, *285*, 41-75, 1998.

D. Dong, Jet Propulsion Laboratory, MS 238-332, 4800 Oak Grove Drive, Pasadena, CA 91109. (dong@freia.jpl.nasa.gov)

P. Fang, Scripps Institution of Oceanography, Scripps Orbit and Permanent Array Center (SOPAC), Cecil H. and Ida M. Green Institute of Geophysics and Planetary Physics, La Jolla, CA 92093-0225. (pfang@ucsd.edu)

D. D. Jackson, Z.-K. Shen, and A. Yin, Department of Earth and Space Sciences, University of California, Los Angeles, 90095-1567. (djackson@ucla.edu; zshen@ess.ucla.edu; yin@ess.ucla.edu)

Y. Li and C. Zhao, First Crustal Deformation Monitoring Center, China Seismological Bureau, Hedong District, Tianjin, China. (djzl@shell.tjvan.net.cn; ckzhao@371.net)

(Received December 28, 1998; revised September 22, 1999; accepted November 3, 1999.)